Nanopore sensors for nucleic acid analysis

2003 J. Phys.: Condens. Matter 15 R1365

(http://iopscience.iop.org/0953-8984/15/32/203)

INSTITUTE OF PHYSICS PUBLISHING JOURNAL OF PHYSICS: CONDENSED MATTER

J. Phys.: Condens. Matter **15** (2003) R1365–R1393 PII: S0953-8984(03)58447-8

TOPICAL REVIEW

Nanopore sensors for nucleic acid analysis

Jonathan J Nakane[1], **Mark Akeson**[2] **and Andre Marziali**[1,3]

[1] Department of Physics and Astronomy, University of British Columbia, 6224 Agricultural Road, Vancouver, V6T 1Z1, Canada
[2] Howard Hughes Medical Institute and Department of Chemistry, University of California, Santa Cruz, CA, USA

E-mail: andre@physics.ubc.ca

Received 17 January 2003
Published 1 August 2003
Online at stacks.iop.org/JPhysCM/15/R1365

Abstract

In the past decade, nanometre-scale pores have been explored as the basis for technologies to analyse and sequence single nucleic acid molecules. Most approaches involve using such a pore to localize single macromolecules and interact with them to garner some information on their composition. Though nanopore sensors cannot yet claim success at deoxyribonucleic acid (DNA) sequencing, nanopore-based technologies offer one of the most promising approaches to single molecule detection and analysis. The majority of experimental work with nanopore detection of nucleic acids has involved the α-haemolysin (alpha-HL) ion channel—a heptameric protein with a $\sim$2 nm diameter inner pore which allows translocation of single-stranded DNA. Analysis of externally induced ion current through the pore during its interaction with DNA can provide information about the DNA molecule, including length and base composition. This review focuses on alpha-HL and its applications to single-molecule detection. Modified alpha-HL and other biological and synthetic pores for macromolecule detection are also discussed, along with a brief summary of relevant theoretical work and numerical modelling of polymer–pore interaction.

(Some figures in this article are in colour only in the electronic version)

Contents

[3] Author to whom any correspondence should be addressed.

1. Introduction

Despite the large amount of information that has become available from the Human Genome Project and other genome-wide deoxyribonucleic acid (DNA) sequencing projects, it is clear that an even larger amount of information will need to be gathered to fully utilize the sequence obtained to date. For example, functional analysis of the genome will require sequencing the DNA of many other organisms of varying evolutionary proximity to humans. Each mammalian genome is approximately the same size as the human genome, which cost approximately $300 million [1] to sequence using standard Sanger sequencing methods [2].

This demand for faster and cheaper technology is in part responsible for the expansion of research in methods aimed at analysis of single macromolecules. At present, much of the time and cost required to analyse biological macromolecules such as DNA is expended in making and purifying many copies of these molecules to provide sufficient signal-to-noise ratios for fluorescence-based detection schemes. Direct analysis of single molecules would obviate the need for much of this upstream work. Single molecule methods may also provide unique gene expression information by allowing analysis of nucleic acids from single cells, instead of averaging over many cells.

Many approaches to single-molecule analysis of macromolecules have been pursued. Optical tweezers and traps [3–9], steady shear flow [10], combinations of optical trapping and mechanical actuators [11], oscillating non-uniform electric fields [12], magnetic tweezers [13, 14], biomembrane force probes [15], atomic force microscopy (AFM) methods [16, 17], single-molecule fluorescence detection [18, 19] and fluorescence resonance energy transfer (FRET) probes [20] have been used to study the mechanical properties of biological polymers [21]. Attempts to directly size or determine the composition of individual nucleic acid fragments have also been made by flow cytometry [22], optical mapping [23], and capillary electrophoresis (CE) separation with single-molecule detection [24, 25]. Fluorescence detection of single immobilized molecules has been used to detect specific sequences within a DNA strand [26, 27], while FRET probes have been proposed as a possibility for direct sequencing [28, 29]. However, none of the single-molecule methods used to date has been capable of sequencing significant numbers of nucleotides on single DNA molecules.

In the past decade, nanometre-scale pores have been explored as the basis of technologies for single-molecule sequencing and analysis. Most of these involve using such a pore to localize and interact with single macromolecules to garner some information on their composition. Though nanopore sensors cannot yet claim success at DNA sequencing, nanopore-based technologies offer perhaps the most promising approaches to single-molecule detection and analysis.

Nanopores can be applied in their simplest form as Coulter counters (Beckman Coulter, Fullerton, CA), where macromolecules carrying a net electrical charge are electrophoretically driven through the nanopore by an applied electric potential across the pore. Macromolecules entering the pore produce measurable transient drops in the ionic current through the pore that

can be monitored to determine the number of molecules passing through the pore and used to estimate the local macromolecule concentration [31]. This least technically challenging use of nanopores may result in the first practical applications of this technology. Reviews of Coulter counters and similar applications of biological channels can be referred to for more information [31, 32].

The characteristic that makes nanopores useful for analysis of individual macromolecules is that the scale of the pores is the same as the molecules of interest. For example, the diameter of single-stranded DNA (ssDNA) is approximately 1.3 nm, while the diameter of the narrowest restriction in α-haemolysin (alpha-HL) protein, the most commonly used organic pore for DNA analysis, is approximately 1.5 nm. For ssDNA to pass through this channel, the molecule must be straightened from its randomly coiled native state, with the individual nucleotides entering and exiting the channel in single file. This serial progression of the nucleotides makes nanopores very attractive for direct DNA sequencing schemes. The alpha-HL protein has been the mainstay of nanopore-based detection of nucleic acids, largely as a result of its ideal inner pore diameter, suitable internal geometry and low current noise due to the absence of spontaneous gating. Seminal work by Kasianowicz *et al* [33] demonstrated that physical blockage of ion current through this pore during translocation of a nucleic acid molecule can be used to partially characterize the molecule.

Though nanopore analysis of macromolecules has hitherto been performed primarily with biological pores of insufficient stability for instrumentation purposes, the development of synthetic pores with nanometre-scale dimensions [34, 108, 110] opens up the possibility of developing microfabricated instrumentation based on synthetic nanopores with similar behaviour to their biological counterparts. This could allow for completely electronic detection of analytes to be performed on miniaturized, microfabricated devices [35].

Several efforts are under way to bring to fruition the most ambitious nanopore application—direct, single-molecule sequencing of DNA. This has been proposed [36–38] as a possibility based on experience with alpha-HL. Though it is not clear if ionic current measurement methods used to date will be capable of single-nucleotide resolution, several groups have proposed methods to couple nanopore technologies with other detection schemes such as electrical dipole measurements [39], near-field spectroscopy [40] and FRET fluorescence [28, 29] to achieve this ambitious goal.

As most of the experimental work to date for nanopore-based nucleic acid analysis is based on the alpha-HL pore, this review will focus on this organic pore and its applications to single-molecule detection. Modified alpha-HL and other biological and synthetic pores for macromolecule detection will also be discussed followed by a brief summary of relevant theoretical work and numerical modelling of polymer–pore interaction. A more in depth look at the theoretical treatment of polymer–nanopore interactions can be found in an excellent review by Meller [113].

2. *Staphylococcus aureus* α-haemolysin structure and properties

Alpha-HL is a 293-residue water-soluble protein monomer that self-assembles as a heptamer in cell membranes and synthetic lipid bilayers to form a 1.5 nm diameter aqueous channel through the membrane [41]. The protein is secreted by the human pathogen *Staphylococcus aureus* and binds to and lyses human platelets by making their membranes permeable to water, ions and low molecular weight molecules.

The structure of alpha-HL has been determined by crystallography to 1.9 Å resolution [41]. The resulting image (shown in figure 1) shows a 10 nm long mushroom-shaped heptamer. The transmembrane domain of the channel comprises a 14-strand beta barrel with a hydrophilic

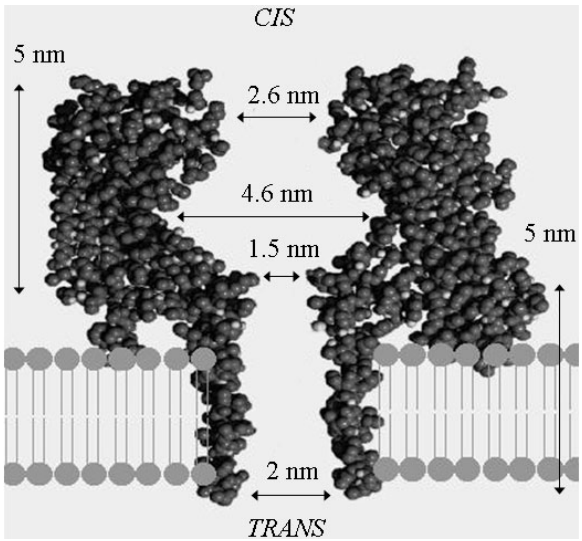

Figure 1. A single alpha-HL channel is shown in cross section embedded in a lipid bilayer. Image adapted from [55] with permission. ©2000, Elsevier Science.

interior and hydrophobic exterior. Following the channel orientation adopted in most experiments, the mushroom-shaped 'head' of the molecule will be referred to as the *cis* side, and the stem end as the *trans* side.

The aqueous channel [41] contained in the pore cross section (see figure 1) is composed, from *cis* to *trans* side, of a 2.6 nm diameter 'mouth', a 4.6 nm maximum diameter 'vestibule', a 1.5 nm diameter 'limiting aperture', followed by a 5 nm long stem approximately 2 nm in diameter. There are many charged residues in the pore at neutral pH, most notably a ring of positively charged lysines (K147) interposed with a ring of negatively charged glutamates (E111) at the limiting aperture.

Electrical behaviour of the channel in electrolyte solutions shows Ohmic characteristics with conductivity linearly proportional to electrolyte ion concentration, and current linearly proportional to voltage though with some rectification and mild selectivity for anions [41]. In 1 M KCl solution, 120 mV potential from *trans* to *cis* results in a current of 120 pA, while the same potential applied *cis* to *trans* results in approximately 90 pA of current [42].

Current noise characteristics of the channel are dependent on the pH of the solution, presumably due to reversible protonation of residues in the pore leading to changes in the effective size of the aqueous channel and consequently changes in its conductance [43]. Measurements of noise spectral density [43] as a function of pH and pD in H_2O and D_2O indicate several residues in the channel with pK of approximately 5.5, leading to a maximum value of noise spectral density near a pH of 6.

Dimensions of the aqueous channel inside alpha-HL have also been probed by applying various polymers of known molecular weights and hydrodynamic radii to each side of the pore and observing the change in channel conductance to determine to what extent the pore is explored by the polymers [44]. Though the details of the interior of the pore could not be observed with this measurement, the experiment confirmed the presence of a channel opening at each end of the pore of virtually identical diameters (2.4–2.6 nm) with a restriction of 1.8 nm diameter detected from the *cis* side of the pore, and a restriction of 1.2–1.4 nm diameter detected from the *trans* side of the pore. These dimensions agree well with the narrow part of the

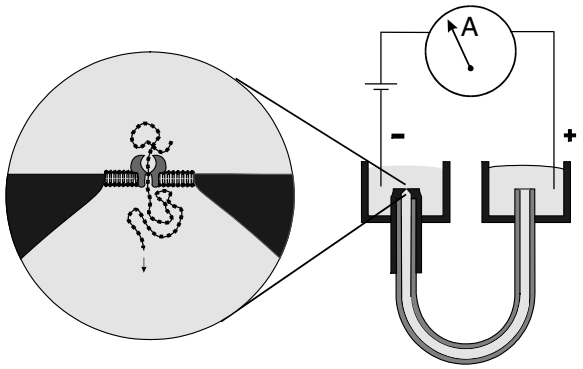

Figure 2. Supporting apparatus for horizontal bilayer experiments. A U-shaped Teflon® patch tube connects two baths milled into a Teflon support (left). One end of the Teflon® patch tube has a conical tip that narrows to a 25 μm aperture (right). Lipid bilayers are formed across this aperture, and alpha-HL channels are inserted into the bilayer. Nucleic acids are driven through the alpha-HL channel by an applied voltage of 50–350 mV, positive on the *trans* side. Reprinted from [51] with permission. ©1999, the Biophysical Society.

mouth and with the limiting aperture of the pore respectively, as indicated by crystallography measurements.

2.1. Native α-haemolysin sensor applications

Experiments with alpha-HL have provided groundbreaking demonstrations of the sensor possibilities provided by nanopores. Alpha-HL channels were the first channels used [33] to demonstrate detection and characterization of single nucleic acid molecules by ion-current detection. Apparatus and methods similar to those used for this initial work continue to be relied upon and are therefore presented in some detail.

2.1.1. Equipment. Ion channel experiments require low electrical noise to accurately detect picoamp-level currents, and extreme cleanliness in the wetted parts of the apparatus to allow reliable formation of bilayers and organic pores. These constraints dictate in part the typical horizontal bilayer experimental layout shown in figure 2. Two small reservoirs machined (typically) from a single Teflon® block are connected by Teflon® heat-shrinkable tubing (double-walled PTFE tubing, EW-95810-00, Cole-Parmer). One end of the tubing serves as the support for the lipid bilayer and protrudes into the *cis* chamber. The other end of the tubing is connected to the bottom of the *trans* chamber. The tubing is typically of internal diameter (ID) 0.065 inches, but can shrink with heat to completely constrict. In one approach, heat shrinking and internal melting of the Teflon® is relied on to shrink the ID of the tubing to approximately 25 μm by using thin steel wire as a mandrel. Careful removal of the wire and trimming of the shrunk Teflon® tube results in a 25 μm opening that now separates the two fluid reservoirs. The opening is located at the end of the Teflon® tube in the *cis* chamber and is easily accessible from above for both manual and microscope access. After cleaning by boiling in nitric acid and thorough rinsing, the 25 μm orifice is coated with a thin layer of phospholipid. The Teflon® reservoirs and tubes are then filled with electrolyte—typically buffered 1 M KCl, and a lipid bilayer (diphytanoyl-PC (Avanti Polar Lipids)) is formed across the 25 μm orifice, electrically separating the two reservoirs.

Silver chloride electrodes are inserted in both reservoirs and are connected to an Axopatch 200B (Axon Instruments, Foster City, CA) patch clamp amplifier with a Peltier-cooled headstage. Currents in the picoamp range are easily measured with this instrument. Root mean square (rms) noise in the current is typically $\sim$1 pA_{rms} at DC using a 5 kHz bandwidth filter, with the entire apparatus (including the amplifier headstage) housed in an electromagnetic shielding enclosure. Typically, 100 mV is applied across the bilayer—potentials greater than $\sim$400 mV cause the bilayer to rupture. Once a potential is set up across the lipid bilayer, alpha-HL (Calbiochem) is added to the *cis* reservoir. Incorporation of a single alpha-HL channel is detected as a stepwise increase in the ionic current, with each properly incorporated channel resulting in approximately 100 pA per 100 mV of applied potential. Flushing the *cis* chamber with fresh electrolyte solution immediately after the first increase in current prevents incorporation of additional channels. Though flawed channels do occasionally incorporate, yielding currents with a lower conductance, the proper heptamer channels can be distinguished by the rectifying characteristics stated above.

Once a single channel has incorporated and is deemed to be stable, analyte molecules can be placed in the *cis* reservoir and allowed to diffuse to the pore for detection. Since these molecules are typically nucleic acids and thus negatively charged in solution, the *cis* chamber contains the cathode, so that the applied potential transports negatively charged molecules from *cis* to *trans* through the pore. Translocation events can then be recorded as transient decreases in current measured with the Axopatch amplifier.

2.1.2. Seminal experiments. The earliest efforts resulting in detection of DNA translocation through an ion channel were performed independently by George Church at Harvard [36, 37, 45] and by Kasianowicz *et al* [33]. The initial work performed at Harvard employed lambda phage to insert double stranded DNA through an ion channel into a cell. Patch-clamp techniques [46, 47] were used to detect the decrease in ion current as the DNA was electrophoretically forced through the channel. The first single-molecule detection of nucleic acids using alpha-HL channels was performed by Kasianowicz *et al* [33]. This work employed a single alpha-HL pore to achieve high signal to noise detection of polyuridylic acid (poly(U)) of lengths ranging from 100 to $\sim$500 nucleotides (nt) as well as synthetic ssDNA 150 nt in length with sequence containing A, C and T in a pattern designed to minimize formation of secondary structures. Experiments were also performed with poly(A), poly(C), poly(dT) and poly(dC). Figure 3 represents sample current blockages resulting from interaction of poly(U) (average length 210 nt) with the alpha-HL pore. A histogram of the blockage duration times for this polymer, ranging from 100 μs to over 2 ms is shown in figure 4.

As is evident from figure 4, blockage duration times appear to fall into three distinct events for the same polymer. Very short-lived blockages are thought to result from collisions between the polymer and the mouth of the alpha-HL pore without subsequent translocation. The existence of the other two different Gaussian populations of translocation times with different means and variances for the same polymer was tentatively explained as a possible dependence of translocation time on the nucleic acid strand direction during translocation. It was hypothesized that 3′ to 5′ translocation might differ from 5′ to 3′ translocation, though a physical basis for this was not suggested. Recent theoretical work suggests that these peaks may be a result of the pore geometry in conjunction with the orientation of the translocating polymer [48].

To confirm that the blockages depicted in figure 3 result from actual translocations of molecules from the *cis* chamber to the *trans* chamber, competitive polymerase chain reaction (PCR) [49] was employed. Sample was extracted from the *trans* chamber, PCR amplified, size separated by gel electrophoresis, and the results quantified by staining the PCR products

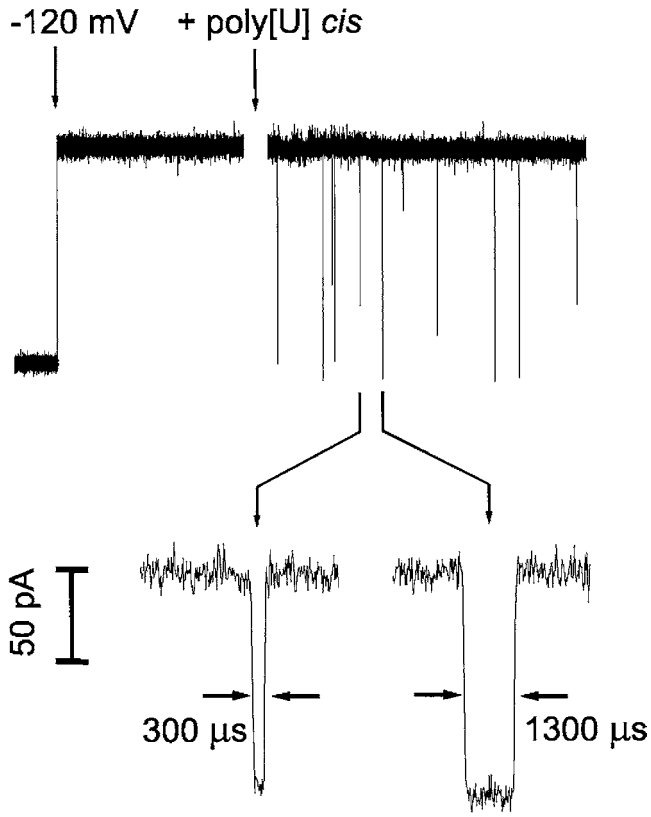

Figure 3. Oligomers of poly(U) caused transient blockades in the alpha-HL single-channel current. At the first arrow, a potential of −120 mV is applied across the membrane (*cis* side negative). This voltage causes a continuous current of −120 pA to flow. At the second arrow, poly(U) of mean length 210 bases is stirred into the *cis* compartment, causing short-lived current blockades. The inset (expanded timescale) shows two typical blockades with lifetimes of 300 and 1300 ms. Reprinted from [33] with permission. ©1996, National Academy of Sciences of the USA.

with SYBR Green—a fluorescent intercalating dye. Results confirmed that the 120 nt ssDNA molecules dispensed in the *cis* chamber in fact translocated to the *trans* chamber, and that the total number of events detected in the two Gaussian peak distributions roughly equalled the number of molecules detected in the *trans* chamber by PCR [33].

The average duration of the current blockages was measured for molecules of different lengths and for different applied voltages, revealing that the mean duration of peaks 2 and 3 in figure 4 varies linearly with molecule length, and inversely with the square of the voltage (although analysis at larger applied voltages shows nonlinear dependence on blockage duration and polymer velocity [50]), while peak 1 appears to be insensitive to changes in the length of the polymer, further substantiating the hypothesis that this peak does not represent translocation of the molecule.

It was also observed that short (∼200 nt) nucleic acid fragments produce more frequent blockage events than an equal concentration of longer (∼1000 nt) fragments [33]. Taking advantage of this effect, it was shown that the alpha-HL pore could be used as a monitor for hydrolysis of polynucleotides. Incubating long (∼1100 nt) poly(U) fragments with ribonuclease-A (an enzyme that cuts poly(U) into shorter fragments) results in a dramatic increase in the rate

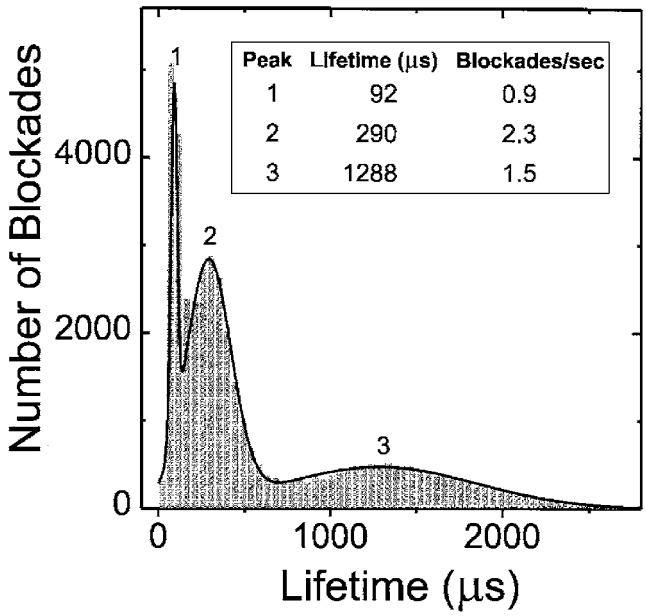

Figure 4. Characteristic lifetimes of channel blockades caused by poly(U) (0.1 mg ml^{-1}, mean length 210 nt, 120 mV), falling within three well-defined peaks. The mean lifetimes corresponding to the three peaks were determined by fitting the sum of three Gaussians to the data. Reprinted from [33] with permission. ©1996, National Academy of Sciences of the USA.

of blockage events in the alpha-HL pore as the long poly(U) fragments are degraded. This increase results partly from the increasing concentration of short fragments as degradation proceeds, and partly from the increasing likelihood of capture of the shorter fragments.

The same methods used to detect individual nucleic acid molecules in these first experiments have been applied to discriminate among single nucleic acid molecules with differing nucleotide compositions [51, 52]. Ion current blockages in alpha-HL caused by RNA homopolymers poly(A)150, poly(C)125, poly(U)150, and by DNA homopolymer poly(dC)100 can be distinguished by the combination of the depth of the current drop and the duration of each blockage event (see figure 5) [51].

Evidence that current blockage signatures can distinguish nucleotide composition within a single molecule is observed using the copolymer $A_{(30)}C_{(70)}Gp$ (see figure 6) [51]. Each event shown in figure 6 begins with a 95% blockage followed by a step increase to an 85% current blockage. These current levels coincide with those of the homopolymer blocks poly(C) and poly(A) respectively, leading to the conclusion that a measurement of ion current blockage is capable of distinguishing the nucleotide composition of a single molecule with a resolution of at least 30 nt. It has also been demonstrated that it is possible to distinguish specific blockage signatures between DNA polymers $poly(dA)_{100}$ and $poly(dC)_{100}$, as well as between polymers comprising repeating dAdC units (e.g. $poly(dAdC)_{50}$) and di-block polymers $poly(dA_{50})(dC_{50})$ and others [52]. Polymer blockage signatures are analysed and identified primarily on the basis of the blockage duration, though small changes in blockage amplitude are also noted. Table 1 lists the translocation properties for some of the polymers tested in this study. These parameters are average values taken from large populations of polymer blockage events. Individual blockage events for populations with similar average parameters (e.g. $poly(dAdC)_{50}$ and $poly(dA_{50})(dC_{50})$) cannot be distinguished

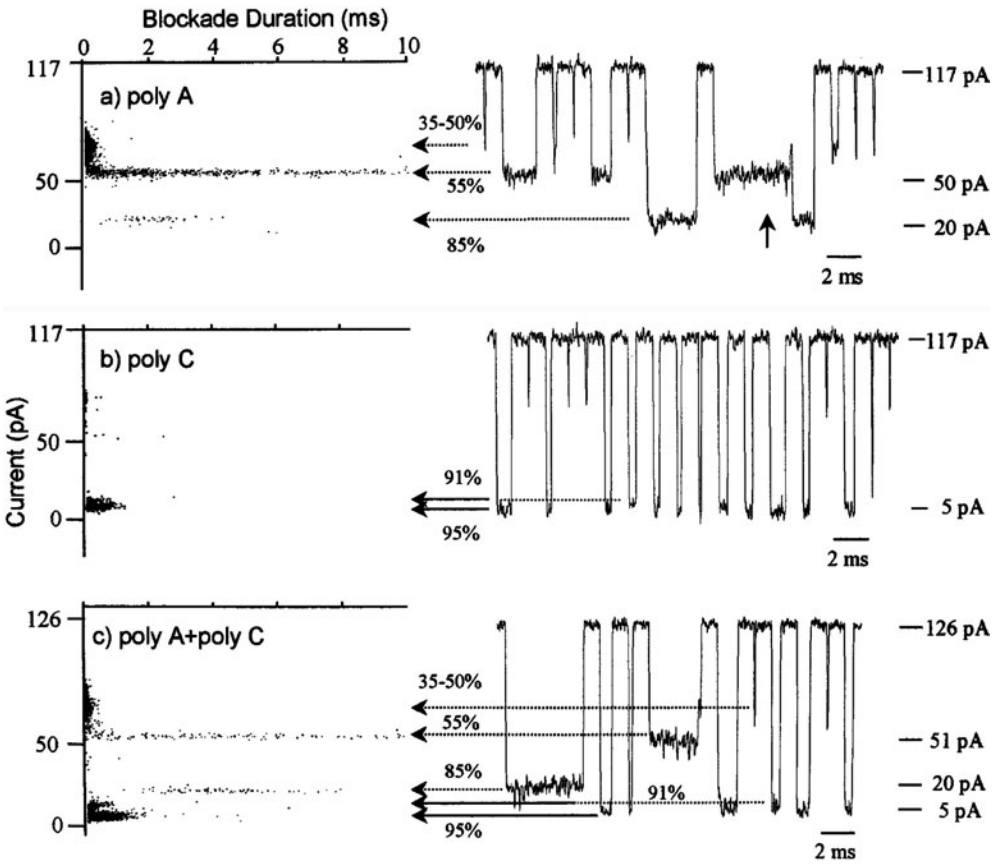

Figure 5. Scatter plots of amplitude and duration of current blockades caused by RNA homopolymers passing through the alpha-HL pore. Typical blockade events comprising each plot are shown on the right. (a) Blockades caused by poly(A) (150 nt mean length, 200 mg ml^{-1}). (b) Blockades caused by poly(C) (125 nt mean length, 200 mg ml^{-1}). (c) Blockades caused by a mixture of poly(C) (125 nt mean length) and poly(A) (175 nt mean length). Quiescent periods between events were spliced out of the plots on the right so that numerous blockades could be presented in one figure. Reprinted from [51] with permission. ©1999, the Biophysical Society.

Table 1. Summary of translocation properties of several 100-mer polymers through alpha-HL. Table from [52] with permission. ©2000 National Academy of Sciences of the USA.

Polymer	Peak value in current-blockade histogram	Peak value in translocation diagram (μs)	Temporal dispersion of translocation duration (μs)
$(dA)_{100}$	0.126 ± 0.012	192 ± 10	55 ± 3
$(dC)_{100}$	0.134 ± 0.010	76 ± 4	15 ± 1
$(dA)_{50}(dC)_{50}$	0.128 ± 0.010	136 ± 7	32 ± 2
$(dAdC)_{50}$	0.141 ± 0.011	177 ± 9	38 ± 2
$(dC)_{50}(dT)_{50}$	0.140 ± 0.011	137 ± 7	25 ± 1
$(dCdT)_{50}$	0.144 ± 0.012	82 ± 4	91 ± 5

with much certainty, though homogeneous populations of such polymers are presumably easily distinguished from each other if many blockage events are collected and averaged.

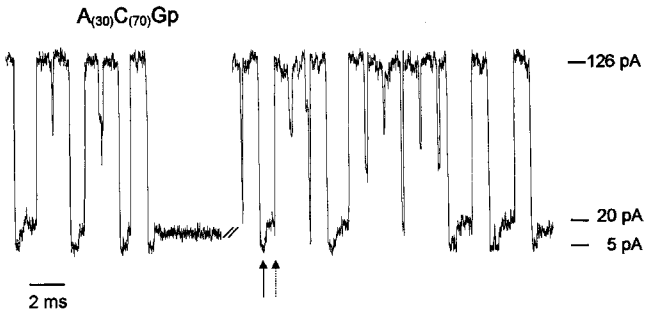

Figure 6. Typical blockades of ion current in the alpha-HL pore caused by $A_{(30)}C_{(70)}$Gp RNA. Most bi-level events first exhibited 5 pA residual current (95% current blockade, solid arrow) followed by a 19 pA residual current (85% blockade, dashed arrow), interpreted as the poly(C) segment at the 3′ end of the molecule entering the pore first. The opposite orientation constituted 10% of the bi-level blockade events. Quiescent periods between events were spliced out so that numerous blockades could be presented in one figure. Reprinted from [51] with permission. ©1999 the Biophysical Society.

It is surprising that these experiments clearly indicate that poly(C) produces deeper blockages than poly(A), given that cytosine is a smaller molecule than adenine. It has been hypothesized [51] that poly(C) may lead to a deeper blockage due to it adopting a single-stranded helical structure [53] while passing through the limiting aperture of alpha-HL.

2.2. Direct sequencing

Step-like signatures in the current blockage caused by translocation of copolymers as shown in figure 6 raise the possibility of direct sequencing [38, 54, 55] of individual DNA molecules by single-nucleotide resolution of current blockage. However, it is unlikely that ion current detection in alpha-HL can be used for single-nucleotide resolution sequencing for two reasons:

(1) only ∼100 current-carrying ions are driven through the pore during translocation of an individual nucleotide [55];
(2) the stem region of the alpha-HL pore is approximately 5 nm long, and thus would contain ∼12 nt during nucleic acid strand translocation.

The change in the current amplitude that could potentially result from varying one of the 12 nucleotides occupying the stem would be reduced by averaging over the rest of the nucleotides. While it may be feasible to distinguish among 10-mer block segments of nucleotides, it is unlikely that the single-nucleotide resolution needed for DNA sequencing will be achieved by alpha-HL.

Modification of alpha-HL, or development of shorter synthetic channels, is not likely to improve the prospect for direct DNA sequencing by detection of ion current blockage. A simple approximation [35] for the ion current density in the vicinity of a narrow aperture in a thin membrane indicates that the high current density in the centre of the aperture does not decrease significantly on axis within one aperture diameter of the membrane. The smallest diameter aperture that will allow ssDNA to translocate through it is approximately 1.5 nm. At least 3 nm of the DNA strand will therefore be sampled by the high-current density region, leading to a blockage signal that is averaged over at least 6 nt.

A simple computer simulation [56] of the signal expected from a hypothetical infinitely thin membrane with a 1.5 nm aperture shows amplitude fluctuations in the blockage level due

Table 2. Data for DNA hairpin structures used by Vercoutere *et al* [57]. From [57] with permission. ©2001, Nature Publishing Group.

Predicted hairpin secondary structure	TT T T G:C C:G C:G 5′ 3′ C:G A:T A:T	TT T T G:C C:G A:T A:T A:T 5′ 3′ G:C C:G C:G	TT T T G:C C:G A:T A:T A:T A:T 5′ 3′ C:G T:A	TT T T G:C C:G A:T A:T A:T A:T C:G T:A 5′ 3′	TT T T G:C C:G A:T A:T A:T A:T C:G T:A C:G 5′ 3′	TT T T G:C C:G A:T A:T A:T A:T C:G T:A C:G C:G 5′ 3′	TT T T G:C C:G A:T A:T A:T A:T C:G T:A T:A C:G 5′ 3′	T T T G:C C:G A:T A:T C:G 5′ 3′	TT T T G:C C:G A:T A A G:C C:G 5′ 3′	TT T T G:C C:G A:T A:T G:C 3′ C:G 5′ T:A T:A G:C TC:GT T T
Identity	3 bp	4 bp	5 bp	6 bp	7 bp	8 bp	9 bp	5 bp 3 dT	6 bp A_{14}	Dumb-bell
$\Delta G°$ [a] (kcal mol^{-1})	−3.0	−4.5	−5.6	−8.2	−9.0	−11.4	−12.8	−4.2	−4.3	−11.3
I/I_o [b] (%)	68	64	60	52	47	35	32	62	53	NA

[a] $\Delta G°$ values for hairpin formation were calculated using the DNA mfold server (http://mfold.wustl.edu/~folder/dna/form1.cgi) based on data from SantaLucia [109]. Assume 22 °C and 1 M KCl.
[b] I is the current average for an event shoulder (in pA). I_o is the current average for the open channel (in pA).

to the periodic structure of ssDNA (i.e. nucleotides alternating with backbone structures) in the range of 1 pA rms for an open channel current of ∼100 pA. Given that

(i) the noise level currently achievable in these experiments is on the order of 1 pA rms,
(ii) the blockage fluctuation resulting from differences between nucleotides is likely to be much less than the blockage fluctuation due to the presence of either the nucleotide or backbone in the aperture,
(iii) thermal motion of the nucleotides will add additional noise to the measured current signal,

it seems unlikely that single-nucleotide resolution will be achieved by detection of small changes in the ion current flowing through any nanopore without employing some mechanism to greatly reduce the translocation velocity of the DNA strand, thus allowing noise reduction through time-averaging of the signal.

It appears, therefore, that single-molecule direct DNA sequencing with nanopores will require alternative detection schemes coupled to the pore (such as near-field spectroscopy or FRET fluorescence probes), or with a method of 'ratcheting' the polymer through the pore so that it moves in discrete steps, as is the case for polymerase action.

2.2.1. Single-nucleotide detection. A possible solution to the resolution limit of alpha-HL detection is the possibility of slowing the rate of DNA translocation, or anchoring a DNA molecule in the pore to increase the dwell time of the nucleotides in the high-current region of the channel such that substantial time averaging of the signal can be performed. Single-nucleotide resolution has been achieved in this manner [57] using DNA hairpins to locate a single nucleotide pair near the alpha-HL limiting aperture for a sufficient time to allow a distinguishable blockage signature to be recorded. This detection scheme employs synthetic DNA oligonucleotides designed to form specific secondary structures, in this case a 4 dT loop linking two complementary strands that anneal into a double-stranded region ranging from 3 to 9 base pairs (bp) in length (see table 2). The hairpin loop in these molecules prevents them from translocating through the alpha-HL channels, leading to very long-lived blockage

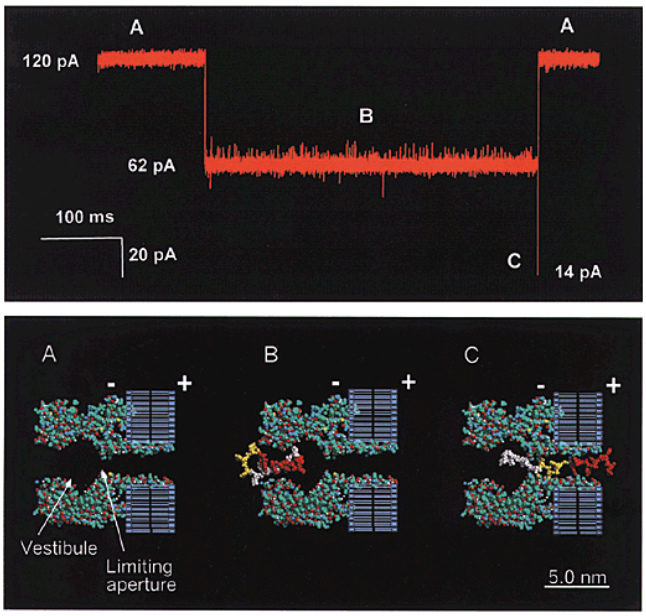

Figure 7. Blockage of the alpha-HL nanopore by a DNA hairpin. The upper panel shows a current trace caused by capture and translocation of a 6 bp DNA hairpin through the pore. The lower panel shows a molecular model of these events. (A) Cross section of the alpha-HL heptamer inserted in a lipid bilayer. (B) Capture of a 6 bp DNA hairpin in the channel causes an abrupt current reduction to an intermediate level ($I/I_o = 52\%$). Because only linear ssDNA can traverse the 1.5 nm limiting aperture, the stem duplex holds the molecule in the vestibule (760 ms median duration at 120 mV applied voltage). The 4-deoxythymidines of the hairpin loop are shown spanning the pore entrance, and the 6 bp of the stem are shown extended into the vestibule. (C) Translocation of the DNA through the limiting aperture of the channel. The partial hairpin blockade ends with a sharp downward spike to ~14 pA ($I/I_o = 12\%$) that lasts about 60 μs. Reprinted from [57] with permission. ©2001, Nature Publishing Group.

states (up to 300 s). It is assumed that the stem (double-stranded section) of the molecule enters the mouth of the pore and is prevented from translocating through the pore either by interaction with the limiting aperture, or by interaction of the loop structure with the mouth of the pore, depending on the length of the molecule (see figure 7(B)). Eventually, the molecule dissociates and passes through the limiting aperture as a single-stranded polymer, leading to the deep blockage expected for ssDNA translocating through the pore. The long duration of the blockages caused by these hairpin molecules allows discrimination between blockage amplitudes for molecules differing in length by a single base pair (see per cent blockage data from table 2). Furthermore, the duration of the blockage event correlates strongly with the standard free energy of the hairpin formation (see figure 8).

Using the blockage duration as a distinguishing parameter, a 6 bp stem molecule d(CGAACGTTTTCGT**T**CG) could be easily distinguished from the same molecule with a single nucleotide difference (6 bp A_{14}—CGAACGTTTTCGT**A**CG). Though the blockage amplitudes for these two molecules are virtually identical, the blockage duration differs by almost two orders of magnitude due to destabilization of the hairpin by the AA mismatch introduced into the stem of 6 bp A_{14}. Though this type of single-nucleotide resolution is not appropriate for large-scale direct sequencing due to throughput limitations, it creates interesting possibilities for mutation detection and measurement of DNA duplex stability.

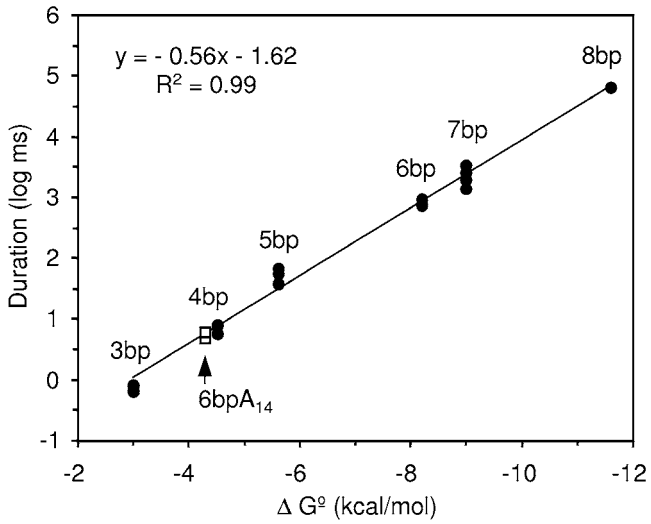

Figure 8. Standard free energy of hairpin formation (see table 2) correlated with median duration of hairpin shoulder blockades (solid circles). Each point represents the median blockade duration for a given hairpin length acquired using a separate alpha-HL pore on a separate day. Median blockade durations and ΔG° for the equivalent of the 6 bp hairpin with a single mismatch (6 bp A14, table 1) are represented by open squares. Reprinted from [57] with permission. ©2001, Nature Publishing Group.

Table 3. Effect of the penultimate base-pair orientation on the dwell time for 9 bp hairpins with different Watson–Crick base-pair termini. Table from [58].

	Penultimate base pair	
Terminal base pair	5′-T • A-3′	5′-A • T-3′
Terminal base pair	Dwell time in lowest level (in milliseconds)	
5′-T • A-3′	7 ± 1	20 ± 4
5′-A • T-3′	43 ± 5	30 ± 6
5′-G • C-3′	160 ± 23	210 ± 90
5′-C • G-3′	50 ± 4	66 ± 20

The composition and orientation of the terminal base pair in the stem of hairpin DNA molecules can also be identified by observing the rate with which the terminal base pair dissociates [58]. Dissociation is monitored by analysis of 'spiking' behaviour observed in the ion current blockage signal. Since the double-stranded stem of the hairpin is too large to penetrate the limiting aperture of alpha-HL, it is hypothesized that dissociation of the terminal base pair of the hairpin stem leads to a short, single-stranded segment of the stem temporarily entering the limiting aperture and leading to a brief, deeper current blockage. It is believed that this low-frequency toggling pattern is a result of interaction between the terminal base pair of the hairpin stem and amino acids on the inside of the alpha-HL channel. The characteristic dwell time of the molecule in its lowest conductance state also provides a means of discriminating not only among the four possible combinations for the terminal base pair, but also among different combinations and orderings of the penultimate base pair (see table 3).

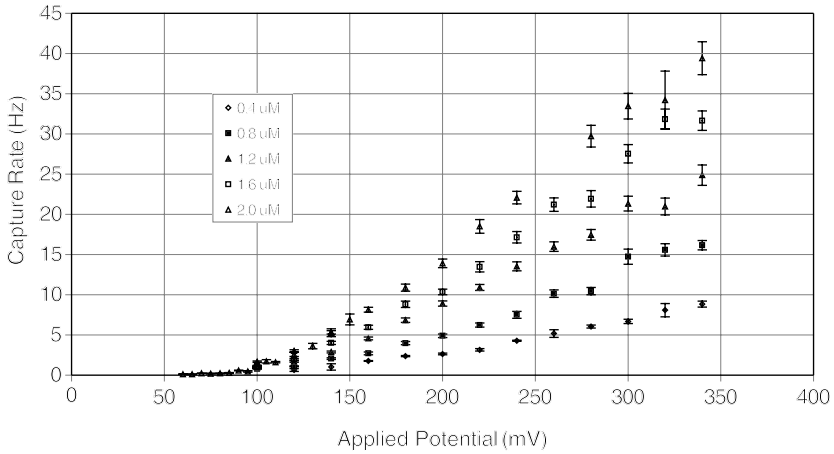

Figure 9. Measured capture rate as a function of voltage applied to the pore for various concentrations of single-stranded poly(dA) (mean length 50 nt) in 1 M KCl. Data below 100 mV were only taken at 2 μM concentration. Reprinted from [35] with permission. ©2002, Wiley–VCH.

2.2.2. Coulter counter applications. The great challenges involved in developing direct sequencing applications of nanopore sensors has led to the exploration of simpler uses of this technology. The concept of using nanopores as molecular Coulter counters has been suggested by several groups [31, 33, 35], and demonstrated for detection of RNA hydrolysis [33] as previously described.

Appropriate application of nanopores as Coulter counters requires characterization of the sensitivity of detection. This in turn requires an understanding of the rate at which molecules are captured by a nanopore under various experimental conditions. A 'capture' event can be defined as the observation of a current blockage of comparable depth to the blockage observed during translocation of the molecule being detected. For alpha-HL, any such blockage implies that the polymer being detected has entered the limiting aperture region of the pore. Though it is possible that the polymer will reach this point in the pore and not translocate fully through the pore, this event is deemed to be very unlikely for a large applied potential based on numerical simulations [35, 48]. In any case, if the purpose of the pore is to detect the presence of molecules in solution, translocation is not essential and partial translocation followed by escape is still a valuable indication of the presence of a molecule near the pore and should not be discounted. The capture rate is therefore measured by calculating the time between blockage events [42, 59], in some cases excluding the time duration of the event itself [35] to remove dependence of the rate on the actual time of translocation.

Measurements of capture rate as a function of the concentration of DNA polymers on the *cis* side of the pore yield a linear relationship [33, 35, 42]. This is expected if the collision rate of molecules with the pore is primarily driven by diffusion, and the flux of molecules on a hemispherical surface is therefore $\sim 2\pi\, DdC$, where D is the diffusion constant for the molecule in bulk solution, d is the diameter of the hemisphere, and C is the molecule concentration. Applying standard known values for these parameters, the predicted rate of DNA molecules reaching the pore given a 1 μM concentration in the *cis* chamber is $\sim$3000 min^{-1} whereas only 300 blockage events per minute are measured for an applied potential of 120 mV [42]. This implies that many of the molecules reaching the pore do not enter the pore at these applied potentials.

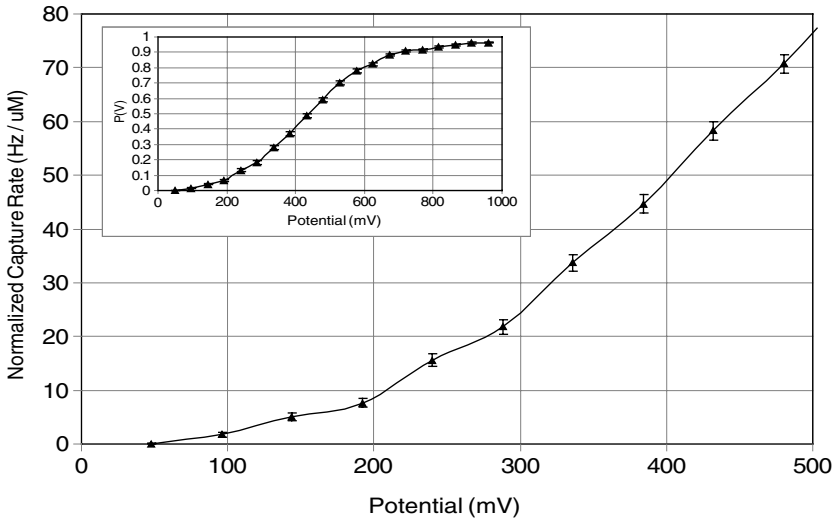

Figure 10. Results of Monte Carlo simulation of a 50-mer translocating through a cylindrical pore. Capture rate is derived from the calculated capture probability $P(V)$ (inset) by scaling with the expected collision rate $R_0 = 4$ DdC, with $D = 5 \times 10^{-11}$ m^2 s^{-1}, yielding a rate of $R_0 = 120$ Hz μM^{-1}. Reprinted from [35] with permission. ©2002, Wiley–VCH.

Measurement of capture rate as a function of applied potential yields two distinct regimes—a low-voltage regime (0–120 mV) within which an exponential dependence of capture rate versus voltage is seen [42], and a separate regime above 120 mV where capture rate increases more gradually with voltage [35, 59] (see figure 9). The change in behaviour of the capture rate versus voltage at approximately 120 mV has been tentatively attributed to polymer–pore interactions, limitations in the capture rate due to the finite translocation time of the polymer, and decreased capture probability due to decreased ionic current during the duration of blockage events [59]. Simple Brownian dynamics simulations (see figure 10) of polymer translocation through a pore [35] yield a similar threshold behaviour without the inclusion of polymer–pore interactions.

Though the alpha-HL–lipid bilayer system as currently used is not capable of withstanding potentials greater than ∼0.4 V before rupturing, extrapolation of the measured capture rates to higher voltages can be performed as an estimate of the detection limit of a hypothetical synthetic pore capable of withstanding larger potentials. Estimates [35] indicate a capture rate of 40 Hz at 500 mV for 1 μM concentration of 50-mer DNA molecules. As noted in the early work [33], smaller molecules appear to lead to higher capture rates [35]. Though 40 Hz for 1 μM concentration appears to be very low sensitivity, it should be noted that this sensitivity is constant regardless of the volume being sampled, which is not the case for many other detection schemes. For volumes on the scale of 100 nm^3 (∼1 molecule at 1 μM), nanopore detectors similar to alpha-HL could lead to a very high detection efficiency.

A DNA sequencing scheme has been proposed [35] based on the molecular Coulter counter concept, through which analyte bands in capillary electrophoresis are detected by a nanopore sensor rather than optical means (see figure 11). Though this scheme would not be particularly sensitive for capillaries at the currently used diameters (50–75 μm), it could become appropriate if submicron-scale capillaries are developed for DNA separation. Incorporation of nanopore detection with CE separation almost certainly requires a synthetic pore for durability and compatibility with separation matrices.

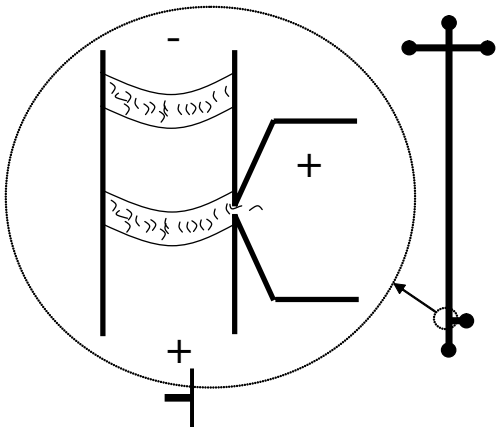

Figure 11. Schematic of proposed separation capillary with nanopore detector (not to scale). An electrophoresis separation potential is applied across the full length of the capillary, while a much smaller capture potential is applied across the pore. Current through the pore is detected and the frequency of events, or capture rate, is plotted as an indicator of local concentration of analyte. As bands of analyte electrophorese past the detector, bursts of events are expected at the nanopore detector. Though the nanopore is shown as fabricated in the capillary wall, it may be more practical to mount the nanopore outside the capillary at the elution end of the capillary. Reprinted from [35] with permission. ©2002, Wiley–VCH.

3. Sensors based on modified α-haemolysin

The inner pore formed by the native alpha-HL protein can be modified via mutation of the amino acid sequence, modification of existing functional groups inside the pore, covalent attachment of molecules to functional groups inside the pore, or by trapping molecules inside the pore. Any of these methods may change the internal characteristics of the pore geometrically, chemically or electrostatically, and provide mechanisms for a greater degree of sensitivity to translocation of particular molecules, including nucleic acids.

ssDNA fragments can be attached to the inside of the alpha-HL pore to allow for the detection of DNA strands via specific hybridization with complementary oligonucleotides [60, 61]. As shown in figure 12, short single-stranded oligonucleotide target strands (5′-CATTCACC-3′) with a hexamethylene linker are covalently anchored to the cysteine-17 group of a monomer alpha-HL unit. Incorporation of one modified and six unmodified units forms a complete heptamer pore with the oligonucleotide target strand just inside the pore vestibule, and reduces the mean open-channel current measured through the pore by ∼30% [61]. When oligonucleotide strands of DNA fully complementary to the target strands are added to the *cis* side under a 100 mV applied potential, partial blockades with durations on the order of hundreds of milliseconds result, followed by short spike-like events with almost complete blockage of the pore and a mean lifetime of 0.2 ms. Non-complementary oligonucleotides passing through the pore result in only the short deep spikes and none of the long-lived partial blockades, presumably since the latter translocate without any hybridization to the target oligonucleotide.

It is also possible to uniquely determine the final three bases in a 9-mer target oligonucleotide tethered to the inside of the alpha-HL pore. This is done by first observing the differences in the duration of the partial blockades from four sets of 7-mer oligonucleotides, with each of the four different nucleotides used at the first position in question, noting which of the four oligonucleotides results in the longest partial blockade duration, and using this 7-mer

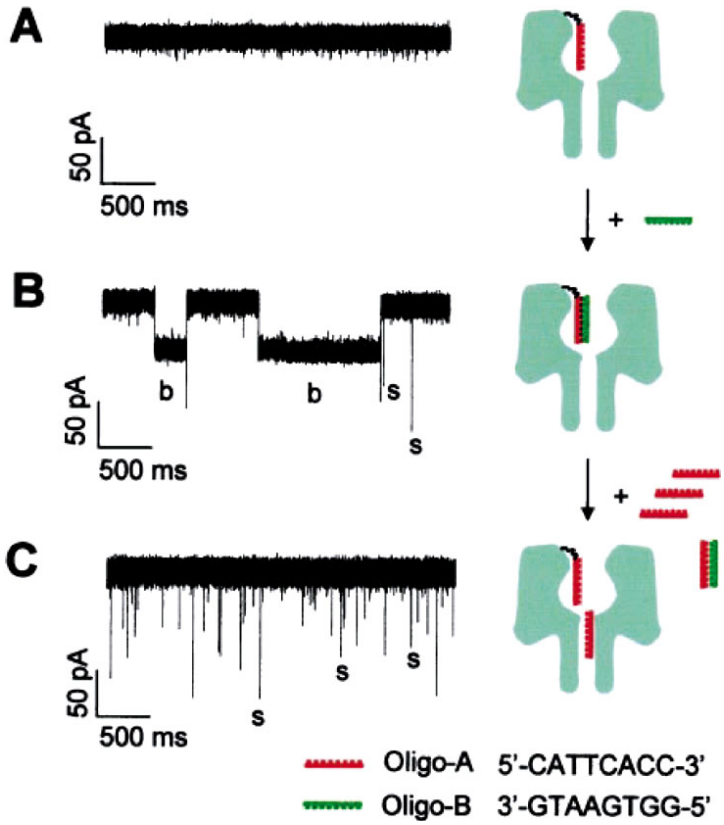

Figure 12. An alpha-HL pore modified with a single DNA oligonucleotide responds to individual binding events with oligonucleotides of complementary sequence. (A) Representative single-channel current trace of the modified alpha-HL with the target oligonucleotide strand, oligo-A, tethered to the inside of the pore at a transmembrane potential of +100 mV relative to the *cis* side of the bilayer. (B) Representative trace of the same channel as in (A) in the presence of the strand complementary to the target oligonucleotide inside the pore. Negative current deflections (b) represent individual binding events of oligo-B (green) to the tethered oligo-A (red). The short downward spikes (s) in the trace are translocation events of oligo-B that did not bind to the tethered oligonucleotide. (C) Trace of the same channel as in (A) and (B) with 67 nM oligo-B and 3.3 nM oligo-A in the cis chamber. Excess oligo-A hybridizes to oligo-B and thereby competes for the binding of oligo-B to the tethered oligonucleotide. The short downward spikes in the trace are translocation events of excess oligo-A molecules through the pore. Reprinted from [61] with permission. ©2001, National Academy of Sciences of the USA.

oligonucleotide strand to work out the next base in the sequence [60]. Further identification of short DNA sequences with engineered nanopores may be possible by incorporating different complementary strands, or other target molecules with nucleotide-specific interactions.

Other modifications to the interior of the alpha-HL pore have been made for the detection of other biomolecules and analytes of interest. Biotin molecules have been tethered to the inside of the alpha-HL pore with a 3.4 kDa polyethylene glycol (PEG) molecule (∼27 nm when stretched) covalently attached to the cysteine-106 group of one monomer unit at a position deep inside the vestibule of the pore [62]. The ionic current through the resulting pore is ∼15% lower than from a typical alpha-HL pore. In addition, high-frequency and high-amplitude negative spikes are observed in the current from the uncharged biotin and

PEG tether translocating repeatedly from the *cis* and *trans* sides due to thermal fluctuations. When streptavidin molecules, which are too large to translocate through the pore, are introduced into the system, they are captured by the biotin molecules and result in distinct changes in the measured ionic current: capture on the *cis* side of the pore results in the PEG tethering molecule being pulled away from the narrowest inner restriction of the pore, allowing almost full conduction through the pore without noise spikes, while capture on the *trans* side of the pore requires the PEG molecule to pass through the inner restriction in the beta barrel, which reduces the current through the pore semipermanently to the average amplitude of the short-lived spikes.

It is also possible to trap molecules very close in size to the pore inner dimensions to provide the steric, chemical or electrostatic interactions required to detect the desired analyte. Cyclic proteins added to the bulk solution pass through the alpha-HL pore with blockades of the order of 2–10 ms, and allow for the detection of even smaller mellitic acids passing through the pore on much shorter timescales based on changes in the measured ionic current–noise characteristics [63]. As a further refinement, it is possible to combine the techniques of site-specific modifications and the trapping of modifier units inside the pore: the addition of two binding site mutations to the narrow beta barrel at the *trans* side of the pore allows for two small cyclodextrins to be lodged inside the pore, creating a small nanocavity ($\sim$4400 Å^3) within the beta barrel where small molecules can be trapped for durations on order of tens of milliseconds, resulting in a measurable decrease in current [64]. A variety of other modifications to the inner pore of alpha-HL have been made to detect other molecules as described in an overview of alpha-HL modifications [32].

3.1. Other organic pores and applications

In addition to alpha-HL, there are other membrane-bound proteins that have been isolated and incorporated into artificially constructed lipid bilayer systems to allow for DNA translocation, and in some cases to monitor the passage and translocation of DNA based on detectable changes in ionic current through the pores.

The voltage-dependent mitochondrial ion channel (VDAC), also called mitochondrial porin, is a 30 kDa mitochondrial membrane protein with an inner diameter of 2.5–3 nm. An individual channel can be inserted into a planar phospholipid layer using a technique similar to that of the alpha-HL method [65, 66]. The addition of double-stranded DNA segments (633 bp) to the solution with an applied transmembrane voltage results in a measurable decrease in the mean ionic current and a change in the current noise. Analysis of the *trans* solution via PCR after each experiment confirmed that DNA had in fact translocated through the pore [66], although there is no indication that individual polymer units could be counted and identified by only monitoring the ionic current. Different binding sites inside the VDAC pore may account for differences in noise characteristics that are observed for different nucleotide types [65].

Similarly, the bacterial ion channels contained in the membrane vesicles of *Bacillus subtilis* inserted as single channels into phospholipid bilayers were found to translocate 4.2 kb double-stranded plasmids. This resulted in a detectable reduction of the mean current and increase in noise of the measured channel current [67]. Translocation was again verified using standard PCR, but without an indication that individual molecules could be detected or counted from current measurements alone.

A nucleic acid binding/channel protein (NAC) purified from rat renal brush border membranes is used to detect single-stranded 20-base long DNA [68]. Once a single NAC is incorporated into an artificial lipid membrane, no channel current is detected without the presence of nucleotides; however, the addition of 20-mer oligonucleotides to the solution

results in detectable pulsing in the channel current on the order of 1–2 pA at 100 mV in buffered 200 mM CsCl, with clear transitions between the closed and open state of the channel. Radioactively labelled oligonucleotides were used to confirm translocation across the bilayer, although the correlation between DNA present in the *trans* side and the event rate in the measured ionic current was not examined.

In one application of nanopores used for analyte detection not involving translocation of the molecule being detected, gramicidin pores are modified with the addition of streptavidin binding sites to the pore and the attachment of biotinylated oligonucleotide probes ranging from 15 to 23 bases in length [69]. Although gramicidin pores are not large enough to translocate DNA directly, when target oligonucleotides with regions complementary to the probe sequences are added to the solution, conduction through the gramicidin pores turns off, allowing for real-time measurement of the forward and reverse reaction rates of oligonucleotide hybridization.

3.2. Synthetic nanopores and supporting structures

Though alpha-HL nanopores have almost ideal properties for detection and limited identification of individual nucleic acid strands, the time and expertise required to form a single channel, and the limited lifetime (5 min–24 h) and fragility of the conventional artificial lipid bilayer system, make it an unlikely commercial device. Possible alternatives include synthetic channels with properties similar to alpha-HL, or more robust organic channels in stable membranes.

3.2.1. Supporting membranes. It may be possible to incorporate an organic nanopore in a commercially available instrument if the pore–bilayer combination was made more robust. One approach is the use of smaller orifices on which to form the artificial lipid bilayer. Whereas present methods using Teflon® shrink tubing have orifices of the order of $\sim$25 μm, materials such as track-etched membranes and free-standing silicon oxide or silicon nitride layers (both discussed below) can be made with orifices on the order of 1 μm or less, allowing for the formation of a much smaller lipid bilayer that could remain intact for substantially longer.

Another method that may be used to increase the lifetime of the lipid bilayer is a mechanical scaffold that acts to support the bilayer. There has been some success using the bacterial surface layer (S-layer) protein from the outermost cell envelope component in walled bacteria and archaea to support artificial lipid bilayers [70–72]. These proteins are recrystallized across $\sim$100 μm orifices to provide a supporting surface for lipid bilayer formation and still allow the insertion of alpha-HL protein into the bilayer. Single-channel readings of the ionic current through the alpha-HL pores using this arrangement [72] have been comparable to the current through alpha-HL in unsupported bilayer membranes, implying that the inner region of the pore and the areas most important to ion conduction may not be affected by the addition of the supporting S-layer protein.

3.2.2. Track-etched membranes and gold nanotubes. Track-etched polycarbonate membranes with pore diameters of the order of tens of nanometres are readily available from commercial sources (Whatman Nuclepore, Newton, MA). The track-etch process [30, 73] involves irradiating a solid membrane material, typically of the order of 10 μm thick, with a beam of high-energy nuclear fragments, then chemically etching the tracks to form pores. The technique allows for a high degree of control over the pore size and axial uniformity based on the concentration and exposure time of the etchant. By controlling the flux of nuclear fragments on the membrane surface, a very low density of holes can be formed, enabling localization of

individual tracks by limiting the contact area of the electrolyte to the membrane and looking for current readings consistent with the conduction of a single pore. Alternatively, one pore can be isolated by physically blocking all other pores with an epoxy coating [30].

Although track-etched membranes have been used successfully for size discrimination and filtering of various molecules via hydrostatic pressure and electrophoresis, the use of track-etched pores for detection of individual biomolecules using the Coulter counter effect is unlikely. This is because the length of the individual pores is determined by the thickness of the polycarbonate membrane. The change in electrical impedance from a nanometre-scale particle in a tube of nanometre-scale diameter but micron-scale length is difficult to distinguish over the noise of the signal.

Smaller pore diameters and lengths can be attained by using track-etched polycarbonate membranes as templates for gold nanotubules, formed by plating in gold solution using a chemical reduction process which deposits gold without the use of an external applied electric potential [74]. The size and profile of the gold nanotubules within the membranes is highly dependent on the pH of the gold-plating solution. At low deposition rates, the gold membrane tends to form layers of uniform thickness all along the boundaries of the pore, while at higher rates more gold is layered at the two ends of the pore than on the inner walls of the pore. This results in constrictions at each of the pore mouths that open to an inner chamber with a larger diameter. Nanotubules with molecular dimensions ($<$2 nm) have been obtained using this technique [75] that can detect nanometre-scale complexes [76]. The magnitude of the reduction in current is found to be proportional to the concentration of the complexes in the bulk solution. Thus far, nucleic acids have not been examined using gold nanotubules, and it is not clear whether this measurement would be feasible since all measurements to date have been taken as the net current sampled over a large number of individual pores.

3.2.3. Ion milling. Practical implementation of a nanopore-based instrument will likely involve synthetic nanofabricated pores for increased robustness. In addition, it may be possible to fabricate pores with controlled inner wall properties, or with the addition of functional units or other useful structures in close proximity to the pore, such as nanofabricated electrodes or additional fabricated constrictions to act as geometrical constraints. Present state-of-the-art semiconductor fabrication techniques using photolithography are limited to feature sizes of the order of tens of nanometres [77]. This is larger than would be required for detecting individual oligonucleotides and other nanometre-scale molecules using the Coulter counter effect. In order to achieve feature sizes on the scale required for detection of biomolecules using nanopores, other specialized fabrication techniques must be applied.

Synthetic pores can be fabricated on the scale of 2–5 nm in a Si_3N_4 membrane using an Ar^+ ion beam incident on a pre-thinned sample membrane [34]. This approach is facilitated by an ion-focusing einzel lens and deflection system that is used to detect Ar^+ ions passing through the pore in the membrane, allowing for an extremely sensitive method of simultaneous pore fabrication and detection. During manufacture of these nanopores at room temperature, the flux of the 3 keV argon ions resulted in diffusion of atoms across the surface of the membrane. This resulted in a reduction in the diameter of pre-existing pores, presumably due to diffusion of surface atoms into the pore. When the temperature was reduced to below 5 °C, the incident ion flux resulted in the formation of holes in the membrane. 5 nm holes fabricated using this technique were used to detect the presence of 500 bp double-stranded DNA passing through the pore by observing intermittent current blockades. Based on ionic current measurements and the known conductivity of the electrolyte used in the experiment, it is estimated that the thickness of the pore used in the detection of DNA is $\sim$10 nm.

3.2.4. Other Synthetic Nanopores. Other novel fabrication techniques have recently been demonstrated to be capable of producing pores appropriate for nucleic acid detection. Saleh and Sohn [108] have manufactured 200 nm diameter pores in poly(dimethylsiloxane) (PDMS) using micromoulding techniques. Interactions between these nanopores and λ-phage DNA molecules (48.5 kbp) can be detected as blockages of tens of pA in an open-channel current of approximately 15 nA. Storm *et al* [110] have manufactured 4 nm pores in SiO_2 layers using tunnelling electron microscopy (TEM) beams at approximately 300 kV. These pores were used to detect dsDNA strands less than 1 kb in length.

4. Theoretical models of polymer translocation through nanopores

Various groups have analysed the process by which molecules are captured or translocate through an ion-conducting pore. In the case where the macromolecule dimensions are much smaller than the inner dimensions of the pore, the macromolecule may be modelled as a sphere, and the analysis can follow analytical [78–84] and computer simulation [85–90] studies of ion conduction experiments and dynamics of individual ions. However, in the case of nanometre-scale pores with dimensions on the same scale as those of individual monomer units in polymer chains, more attention has been paid to analytic models and computer simulations that include polymer dynamics and polymer–pore interactions. The discussion below is not meant to be a comprehensive review of the field, but is intended to highlight some of the main scaling attributes and areas of study undertaken to date on this problem.

4.1. Analytic models

Analytic models of polymer translocation used to date have simplified the three-dimensional problem of polymer translocation into a one-dimensional problem by using the number of monomer segments that have translocated through the pore, n, as the relevant translocation coordinate. Starting with an ideal polymer chain with N segments, Sung and Park [91] expressed the total free energy of the polymer chain during translocation, ignoring arbitrary constants, as

$$\mathcal{F}(n) = \tfrac{1}{2}k_{\mathrm{B}}T\ln[n(N-n)] + n\Delta\mu$$

where k_{B} is Boltzmann's constant, T is the temperature and $\Delta\mu$ is the excess chemical potential energy per monomer on the *trans* side relative to the *cis* side.

Lubensky and Nelson [92] demonstrated that the approximation is valid when the polymer relaxation time outside of the pore is much faster than the translocation speed, and when each of the ends outside of the pore is long enough that the change in the free energy resulting from shifting the polymer through the pore by one monomer unit is small compared with the driving force. That is,

$$\frac{k_{\mathrm{B}}T}{Fa} \ll N \ll \left(\frac{k_{\mathrm{B}}Ta}{\eta b^3 v_{\mathrm{p}}}\right)^{1/3\nu}$$

where Fa is the energy corresponding to the applied force F driving the polymer through the pore with a monomer-to-monomer distance a (analogous to $n\Delta\mu$ used by Song and Park), η is the solvent viscosity, v_{p} is the average drift velocity of the polymer and ν is the Flory exponent due to the excluded volume effect of the individual monomers in the chain.

Using a stochastic model to analyse the translocation dynamics of the polymer when the polymer friction across the pore is proportional to the overall chain length, Sung and Park [91]

derive expressions for the polymer translocation time from the *cis* to the *trans* side after starting with one monomer trapped in the mouth of the pore:

$$\tau(\mu^*) = \begin{cases} \dfrac{L^2}{2D}\dfrac{\pi^2}{8}\left(1 + \dfrac{32}{9\pi^2}\mu^*\right) \sim N^{2+v}, & |\mu^*| \ll 1 \\ \dfrac{L^2}{2D}\dfrac{2}{|\mu^*|} \sim N^{1+v}, & \mu^* \ll -1 \\ \dfrac{L^2}{2D}\dfrac{2}{\mu^{*^2}}\exp(\mu^*) \sim N^v \exp(N) & 1 \ll \mu^* \end{cases}$$

where $\mu^* = N\Delta\mu/k_\mathrm{B}T$, D is the polymer chain diffusivity during translocation and L is the length of the entire polymer chain. For polymers under small applied potentials, translocation time scales according to N^{2+v}, as predicted by translocation by diffusion using Rouse dynamics of a self-interacting polymer, while translocation under larger potentials scale with a smaller $1 + v$ exponent. For a polymer translocating against the potential ($1 \ll \mu^*$), the translocation times increase dramatically with the chain length, as expected.

In their own analysis of polymer–pore dynamics, Lubensky and Nelson [92] used the equation for diffusion with drift:

$$\frac{\partial P(x,t)}{\partial t} = D\frac{\partial^2 P(x,t)}{\partial t^2} - v\frac{\partial P(x,t)}{\partial x}$$

where $P(x, t)$ is the probability that a polymer segment of length x has passed through the pore at time t, D is the diffusion coefficient and v is the average drift velocity. By using absorbing boundary conditions ($P(0, t) = P(L, t) = 0$), and by generating a simplified form of the analytic expression, a distribution of first-passage times through the pore was generated; in this case, first-passage times were defined as the time elapsed between the polymer having one end in the *cis* side of the pore and the last monomer unit leaving the *trans* side. The distribution appears to resemble a Gaussian distribution prior to the peak of the distribution, and an exponentially decreasing distribution after the peak.

Lubensky and Nelson also examined the inclusion of a biased sawtooth potential along the pore to model asymmetric polymer–pore interactions with respect to the direction of translocation through the pore. This was done in an attempt to explain the two distinct populations of translocation times found experimentally [33] (see figure 4) when observing nucleic acids passing through alpha-HL, believed to be due to the $3'$ or $5'$ orientations of the oligonucleotide passing through the pore. Although Lubensky and Nelson's analysis was successful in explaining several features of the translocation populations found in experimental data [33], it was not consistent in predicting the diffusion constants and linear diffusive length $l_\mathrm{d} = D/v_\mathrm{p}$ based on the potential. Several mechanisms were suggested to account for these discrepancies, including additional drag forces from counter-ions and solvent drag, inclusion of the access resistance to the pore, fluctuation in the protonation state of the pore, possible distribution in the length of the polymers used in the experiment, and different forms of the total free energy expression due to geometrical or non-electrical effects, among others.

A model proposed by Muthukumar used nucleation theory to find a scaling law for the translocation time of a polymer through a pore [93]. This was done by considering the rate constants for formation of a stable nucleus of monomers on the *trans* side of the pore. Assuming that the rate constant of the addition of each monomer to the *trans* side, k_O, is independent of the number of monomers on either side of the pore, the translocation time of the polymer τ,

with the scaling with polymer length in the long-chain limit scaled as:

$$\tau \sim \begin{cases} \dfrac{N^2}{k_{\mathrm{O}}}, & \Delta\mu = 0 \\ \dfrac{k_{\mathrm{B}}T}{|\Delta\mu|}\dfrac{N}{k_{\mathrm{O}}}, & \Delta\mu \ll 0 \\ \left(\dfrac{k_{\mathrm{B}}T}{|\Delta\mu|}\right)\exp\left(\dfrac{N|\Delta\mu|}{k_{\mathrm{B}}T}\right), & \Delta\mu \gg 0. \end{cases}$$

A further analysis by Muthukumar [94] examined the effect on translocation dynamics with a di-block copolymer composed of two distinct monomer units with two different nucleation rates. It was found that at low driving potential the type of monomer unit first entering the pore has a much stronger effect on the translocation time than the trailing type of polymer, but that the effect is mitigated as the driving potential is increased.

An analytic analysis of polymer translocation through nanopores with a length comparable to the experimental length of the alpha-HL channel was performed by Slonkina and Kolomeisky [111], where timescales for polymer entry, polymer translocation, and polymer escape from the nanopore are examined. For both long polymers, for which the velocity of translocation is nearly constant, and for shorter molecules, where the velocity decreases as polymer length increases, predictions qualitatively agree with the results found experimentally [50].

Although the majority of analytical treatments to date involving polymer–pore interactions have focused on the dynamics of translocation once one end of the polymer is already inside the mouth of the pore, work has also been done to analytically examine the transition from polymers in the bulk aqueous solution to their interaction with the pore and eventual translocation.

de Gennes derived an expression for the time taken for a single end of a polymer to enter into the pore due to concentration gradients without an applied voltage [95], but the analysis begins with the end of the chain already within one radius from the mouth of the pore. In another study involving the examination of end-capture dynamics, Park and Sung completed an analytical analysis of a polymer translocating through a pore while initially constrained inside a spherical vesicle and in the absence of an applied driving potential. They found that the translocation time τ scaled with L^2 when the radius of the confining sphere R was less than the radius of gyration of the polymer R_g, but that τ scaled with L^3 for $R \gg R_g$ [96]. Ambjörnsson *et al* [112] have analysed the dynamics of polymer capture by combining a random-walk estimate of the probability of finding an end segment at the mouth of the pore, with the 1D diffusive translocation of the polymer through the pore, here including a frictional term to account for interaction of the polymer with the inside of the pore. This model displayed the two voltage regimes found experimentally [35, 42, 59], with polymer capture rates at low voltage following an exponential dependence, while at high voltage following a nearly-linear dependence. Computer simulations have also been used to address the initial capture of one of the polymer ends before translocation [35, 97].

Other effects of polymer–pore interactions have been considered [92, 98–100] but are not discussed here.

Recent experiments by Bates *et al* [107] have examined the escape rate of DNA molecules trapped in the alpha-HL pore in the absence of an applied electric potential. This study uncovered two timescales, separated by a factor of 21, for the escape of the nucleic acid from the nanopore, implying that the molecules either escape quickly, driven by thermal fluctuations, or interact strongly with the pore, delaying escape. This interaction is believed to be the cause of the large difference between the translocation rates found experimentally and those estimated using simple diffusion arguments.

4.2. Computer simulations

In addition to analytic models for describing polymer translocation and interaction with a nanopore, computer simulations of varying levels of complexity have also been used to generate predictions about these systems. There are computer simulations which have examined polymer dynamics in free solution [101], in fixed polymer networks [102, 103] or adsorbed to surfaces [104]. As with the analytic models, experimental work with polymers and pores on the same size scale has led to the development of computer simulations with polymer–pore dynamics in three dimensions and under an applied potential.

The simulations by Chern *et al* [105] use a Monte Carlo method consisting of local random kink-jump moves that are accepted or rejected based on the Metropolis criterion. Briefly, the process is as follows: for each Monte Carlo time step, one of the monomers in a chain of length N is chosen at random. If the chosen monomer is not one of the end monomers, the monomer is rotated a random number of degrees about the axis connecting the two nearest-neighbour monomers; if the chosen monomer is at one of the two ends of the polymer, the monomer is placed to a new random position while keeping the monomer–monomer distance fixed. The new position is then evaluated based on the change in the overall position according to the Metropolis criterion:

$$W(\alpha \to \alpha') = \begin{cases} 1, & \text{if } U_\alpha \geqslant U_{\alpha'} \\ \mathrm{e}^{-\beta(U_{\alpha'} - U_\alpha)} & \text{otherwise} \end{cases}$$

where $W(\alpha \to \alpha')$ is the probability that the polymer in state α will be in state α' at the next time step, $\beta = 1/k_\mathrm{B}T$ and U_α and $U_{\alpha'}$ are the sum of all potential energies (electrostatic, hard-sphere interaction, intrapolymer springs, etc) of states α and α' respectively. The kink-jump method has been demonstrated to correctly describe many polymer properties in free solution as predicted by the Rouse model ('pearl necklace'), such as the polymer end-to-end distance, and the linear evolution with time of the mean-square centre of mass displacement [106]. Such models are not without difficulties, as when simulations result in the polymer being placed in very confined regions, such as in polymer networks or in translocations through pores where the polymer must effectively become linear in order to pass through a restrictive region. In these cases there is difficulty in completing the simulation in a tractable time, as kink-jump moves become increasingly difficult in such regions. Computer simulations often simplify the geometry of the polymer and the pore in these confining regions to negate these effects, for example allowing for monomer units with zero radius, or by using simplified straight-walled pores [35, 105].

Chern *et al* used the kink-jump algorithm to compute the mean first-passage time through a pore with a uniform applied external potential starting with one end of the polymer already in the mouth of the pore, and then compared the results with a numerical simulation of the 1D equation used by Sung and Park [91]. The 3D simulation was run until either the polymer retracted back to the *cis* side or until the entire polymer escaped to the *trans* side. The translocation probability distribution, $P(n, t)$, meaning the number of monomers n in a polymer of length N on the *trans* side of the pore at a given time, was recorded and normalized so that $P(n, 0) = \delta(n - n_0)$, where $n_0 = 1$. Comparisons between the numerical results from the 3D simulation and the 1D simulations using the treatment from Sung and Park show that both result in similar Gaussian-like distributions for P with peaks decreasing in amplitude and shifting toward higher n for increasing t. The survival time of the polymer inside the pore, given as

$$p_\mathrm{surv}(t) \equiv \int_0^N P(n, t)\,\mathrm{d}n,$$

was also calculated. From this value, the mean first-passage time, taken to be the mean time that

a polymer survives in the pore before escaping to either the *cis* or *trans* side can be estimated using

$$\tau \equiv \int_0^\infty p_{\mathrm{surv}}(t)\,\mathrm{d}t.$$

A computational simulation by Kong and Muthukumar [48] used a detailed model of the alpha-HL pore based on the known crystal structure and positioning of amino acid residues obtained from protein database records. This allowed for a much more accurate structure of the alpha-HL pore to be included in the simulation, along with charges on the functional groups in the protein pore that can interact electrostatically with the charged polymer. In addition to the standard 'beads-on-a-string' model, a polymer model with side chains at an angle to the backbone was also used to investigate one possible mechanism for the putative difference in the 5′ and 3′ translocation characteristics of the polymer. The simulation was also run on a straight-walled nanopore to examine the effect of the geometry and charge groups present in the alpha-HL model. Langevin dynamics were used to evaluate motion, wherein the interaction of the polymer and its individual monomers with the solvent particles is taken to be the sum of two forces: a frictional force proportional to the individual monomer velocity, and a randomly fluctuating force with a mean value of zero described as a stochastic variable. The equation of motion for each of the monomers in a Langevin analysis is as follows:

$$m\overline{\frac{\mathrm{d}v}{\mathrm{d}t}(t)} = \overline{F(r,t)} - m\beta\overline{v(t)} + \overline{X(t)}$$

where t is the time, m, β and $v(t)$ are the mass, friction coefficient and velocity of the monomer respectively, $F(r,t)$ is the applied forces external to the monomer, and $X(t)$ is the randomly fluctuating force with a mean of zero.

It was found that the geometry of the alpha-HL pore has an effect on the translocation times. That is, while the straight-walled nanopore model generated only one peak in the distribution of translocation times, the alpha-HL pore geometry resulted in multiple peaks, indicating that geometry alone can account for some of the deviations of translocation times from the expected analytic values. It was also found that the addition of charged groups to the inside of the pore increased translocation times. The side-chain model resulted in only a small difference in the translocation times of the two polymer orientations. It is possible that other factors, such as other interactions with side groups not included in the model, would account for the multiple peaks in the translocation time histogram as found by Kasianowicz *et al* [33]. One qualitative observation from the simulation was that increasing the applied potential across the pore occasionally enhanced the entanglement of the polymer inside the vestibule of the pore, resulting in blockages of the pore which lasted much longer than the typical translocation times. This effect is not seen when a nanotube model is used, leading to the hypothesis that the geometry of the alpha-HL alone could provide a local free-energy minimum for the polymer to become trapped.

References

[1] NIH/NHGRI 2000 *International Human Genome Sequencing Consortium Announces Working Draft of Human Genome* Press release http://www.nih.gov/news/pr/jun2000/nhgri-26.htm

[2] Sanger F N S and Coulson A R 1977 DNA sequencing with chain terminating inhibitors *Proc. Natl Acad. Sci. USA* **74** 5463–7

[3] Simmons R M *et al* 1996 Quantitative measurements of force and displacement using an optical trap *Biophys. J.* **70** 1813–22

[4] Bennick M L *et al* 2001 Unfolding individual nucleosomes by stretching single chromatin fibers with optical tweezers *Nature Struct. Biol.* **8** 606–10

[5] Baumann C G *et al* 2000 Stretching of single collapsed DNA molecules *Biophys. J.* **78** 1965–78
[6] Perkins T T *et al* 1994 Relaxation of a single DNA molecule observed by optical microscopy *Science* **264** 822–6
[7] Perkins T T, Smith D E and Chu S 1994 Direct observation of tube-like motion of a single polymer chain *Science* **264** 819–22
[8] Perkins T T *et al* 1995 Stretching of a single tethered polymer in a uniform flow *Science* **268** 83–7
[9] Chiu D T and Zare R N 1996 Biased diffusion, optical trapping, and manipulation of single molecules in solution *J. Am. Chem. Soc.* **118** 6512–13
[10] Smith D E, Babcock H P and Chu S 1999 Single-polymer dynamics in steady shear flow *Science* **283** 1724–7
[11] Liphardt J *et al* 2001 Reversible unfolding of single RNA molecules by mechanical force *Science* **292** 733–7
[12] Asbury C L and van den Engh G 1998 Trapping of DNA in nonuniform oscillating electric fields *Biophys. J.* **74** 1024–30
[13] Amblard F *et al* 1996 A magnetic manipulator for studying local rheology and micromechanical properties of biological system *Rev. Sci. Instrum.* **67** 1–10
[14] Gosse C and Croquette V 1999 Magnetic tweezers: micromanipulation and force measurement at the molecular level *Biophys. J.* **82** 3314–29
[15] Evans E, Ritchie K and Merkel R 1995 Sensitive force technique to probe molecular adhesion and structural linkages at biological interfaces *Biophys. J.* **68** 2580–7
[16] Florin E L, Moy V T and Gaub H E 1994 Adhesion force between individual ligand–receptor pairs *Science* **264** 415–17
[17] Rief M *et al* 1998 The mechanical stability of immunoglobulin and fibronectin III domains in the muscle protein titin measured by atomic force microscopy *Biophys. J.* **75** 3008–14
[18] Enderlein J 1999 Theoretical investigation of aspects of single-molecule fluorescence detection in microcapillaries *Cytometry* **36** 195–9
[19] Van Orden A *et al* 1998 Single-molecule identification in flowing sample streams by fluorescence burst size and intraburst fluorescence decay rate *Anal. Chem.* **70** 1444–51
[20] Zhuang X *et al* 2002 Correlating structural dynamics and function in single ribozyme molecules *Science* **296** 1473–6
[21] Lavery R *et al* 2002 Structure and mechanics of single biomolecules: experiment and simulation *J. Phys.: Condens. Matter* **14** R383–414
[22] Goodwin P M *et al* 1993 Rapid sizing of individual fluorescently stained DNA fragments by flow cytometry *Nucl. Acids Res.* **21** 803–6
[23] Schwartz D C, Li X J, Hernandez L I, Ramnarain S P, Huff E J and Wang Y K 1993 Ordered restriction maps of Saccharoyces-cerevisiae chromosomes constructed by optical mapping *Science* **262** 110–14
[24] Haab B B and Mathies R A 1995 Single molecule fluorescence burst detection of DNA fragments separated by capillary electrophoresis *Anal. Chem.* **67** 3253–60
[25] Haab B B and Mathies R A 1999 Single-molecule detection of DNA separations in microfabricated capillary electrophoresis chips employing focused molecular streams *Anal. Chem.* **71** 5137–45
[26] Anantharaman T S, Mishra B and Schwartz D C 1997 Genomics via optical mapping II: ordered restriction maps *J. Comput. Biol.* **4** 91–118
[27] Wang Y, Huff E J and Schwartz D C 1995 Optical mapping of site-directed cleavages on single DNA molecules by the RecA-assisted restriction endonuclease technique *Proc. Natl Acad. Sci. USA* **92** 165–9
[28] Gilmanshin R and Chan E 2001 Methods of analyzing polymers using a spatial network of fluorophores and fluorescence resonance energy transfer *US Patent Specification* 6253286 (USA: US Genomics, Inc.)
[29] Chan E 2002 Methods and products for analyzing polymers *US Patent Specification* 6355420
[30] DeBlois R W and Bean C P 1970 Counting and sizing of submicron particles by the resistive pulse technique *Rev. Sci. Instrum.* **41** 909–15
[31] Bezrukov S M 2000 Ion channels as molecular Coulter counters to probe metabolite transport *J. Membr. Biol.* **174** 1–13
[32] Bayley H and Martin C R 2000 Resistive-pulse sensing—from microbes to molecules *Chem. Rev.* **100** 2575–94
[33] Kasianowicz J J *et al* 1996 Characterization of individual polynucleotide molecules using a membrane channel *Proc. Natl Acad. Sci. USA* **93** 13770–3
[34] Li J *et al* 2001 Ion-beam sculpting at nanometre length scales *Nature* **412** 166–9
[35] Nakane J, Akeson M and Marziali A 2002 Evaluation of nanopores as candidates for electronic analyte detection *Electrophoresis* **23** 2592–601
[36] Church G *et al* 1998 Characterization of individual polymer molecules based on monomer–interface interactions USA *US Patent Specification* 5,795,782

[37] Baldarelli R *et al* 2000 Characterization of individual polymer molecules based on monomer–interface interactions *US Patent Specification* 6,015,714
[38] Deamer D W and Branton D 2002 Characterization of nucleic acids by nanopore analysis *Acc. Chem. Res.* **35** 817–25
[39] Bokhari S H *et al* 2002 Parallelizing a DNA simulation code for the Cray MTA-2 *IEEE Computer Society Bioinformatics Conference* (Los Alamitos, CA: IEEE Computer Society Press) p 291
[40] Tegenfeldt J O *et al* 2001 Near-field scanner for moving molecules *Phys. Rev. Lett.* **86** 1378–81
[41] Song L *et al* 1996 Structure of staphylococcal α-hemolysin, a heptameric transmembrane pore *Science* **274** 1859–66
[42] Henrickson S E *et al* 2000 Driven DNA transport into an asymmetric nanometer-scale pore *Phys. Rev. Lett.* **85** 3057–60
[43] Kasianowicz J J and Bezrukov S M 1995 Protonation dynamics of the a-toxin ion channel from spectral analysis of pH-dependent current fluctuations *Biophys. J.* **69** 94–105
[44] Merzlyak P G *et al* 1999 Polymeric nonelectrolytes to probe pore geometry: application to the a-toxin transmembrane channel *Biophys. J.* **77** 3023–33
[45] Roth F P 1998 Regulons revealed with gene expression data and studies on DNA sequencing via ion conductance *Doctoral Thesis* Harvard University
[46] Sakmann B and Neher E 1995 *Single-channel Recording* (New York: Plenum)
[47] Hille B 1992 *Ionic Channels of Excitable Membranes* (Sunderland, MA: Sinauer Associates)
[48] Kong C Y and Muthukumar M 2002 Modeling of polynucleotide translocation through protein pores and nanotubes *Electrophoresis* **23** 2697–703
[49] Gilliland G, Perrin S and Bunn H F 1990 *PCR Protocols* ed T J White (San Diego, CA: Academic) pp 60–9
[50] Meller A, Nivon L and Branton D 2001 Voltage-driven DNA translocations through a nanopore *Phys. Rev. Lett.* **86** 3435–8
[51] Akeson M *et al* 1999 Microsecond time-scale discrimination among polycytidylic acid, polyadenylic acid, and polyuridylic acid as homopolymers or as segments within single RNA molecules *Biophys. J.* **77** 3227–33
[52] Meller A *et al* 2000 Rapid nanopore discrimination between single polynucleotide molecules *Proc. Natl Acad. Sci. USA* **97** 1079–84
[53] Arnott S, Chandrasekaran R and Leslie A G W 1976 Structure of the single-stranded polyribonucleotide polycytidylic acid *J. Mol. Biol.* **106** 735–48
[54] Voss D 1999 Gene express *New Sci.* **164** 40–3
[55] Deamer D W and Akeson M 2000 Nanopores and nucleic acids: prospects for ultrarapid sequencing *Trends Biotechnol.* **18** 147–51
[56] Marziali A 2002 personal communication, unpublished
[57] Vercoutere W *et al* 2001 Rapid discrimination among individual DNA hairpin molecules at single-nucleotide resolution using an ion channel *Nature Biotechnol.* **19** 248–52
[58] Vercoutere W *et al* 2003 Discrimination among individual Watson–Crick base-pairs at the termini of single DNA hairpin molecules *Nucl. Acids Res.* **31** 1311–18
[59] Meller A and Branton D 2002 Single molecule measurements of DNA transport through a nanopore *Electrophoresis* **23** 2583–91
[60] Howorka S, Cheley S and Bayley H 2001 Sequence-specific detection of individual DNA strands using engineered nanopores *Nature Biotechnol.* **19** 636–9
[61] Howorka S *et al* 2001 Kinetics of duplex formation for individual DNA strands within a single protein nanopore *Proc. Natl Acad. Sci. USA* **98** 12996–3001
[62] Movileanu L *et al* 2000 Detecting protein analytes that modulate transmembrane movement of a polymer chain within a single protein pore *Nature Biotechnol.* **18** 1091–5
[63] Sanchez-Quesada J *et al* 2000 Cyclic peptides as molecular adapters for a pore-forming protein *J. Am. Chem. Soc.* **122** 11757–66
[64] Gu L-Q, Cheley S and Bayley H 2001 Capture of a single molecule in a nanocavity *Science* **291** 636–40
[65] Rostovtseva T K *et al* 2002 Dynamics of nucleotides in VDAC channels: structure-specific noise generation *Biophys. J.* **82** 193–205
[66] Szabo I *et al* 1998 Double-stranded DNA can be translocated across a planar membrane containing purified mitochondrial porin *FASEB* **12** 495–502
[67] Szabo I *et al* 1997 DNA translocation across planar bilayers containing *Bacillus subtilis* ion channels *J. Biol. Chem.* **272** 25275–82
[68] Hanss B *et al* 1998 Identification and characterization of a cell membrane nucleic acid channel *Proc. Natl Acad. Sci. USA* **95** 1921–6

[69] Lucas S W and Harding M M 2000 Detection of DNA via an ion channel switch biosensor *Anal. Biochem.* **282** 70–9
[70] Schuster B *et al* 1998 Self-assembled α-hemolysin pores in an S-layer-supported lipid bilayer *Biochim. Biophys. Acta* **1390** 208–88
[71] Schuster B *et al* 2001 S-layer ultrafiltration membranes: a new support for stabilizing functionalized lipid membranes *Langmuir* **17** 499–503
[72] Schuster B and Sleytr U B 2002 Single channel recordings of α-hemolysin reconstituted in S-layer-supported lipid bilayers *Bioelectrochemistry* **55** 5–7
[73] Ferain E and Legras R 2001 Pore shape control in nanoporous particle track etched membrane *Nucl. Instrum. Methods Phys. Res.* B **174** 116–22
[74] Wirtz M, Yu S and Martin C R 2002 Template synthesized gold nanotube membranes for chemical separations and sensing *Analyst* **127** 871–9
[75] Kobayashi Y and Martin C R 1997 Toward a molecular Coulter counter type device *J. Electroanal. Chem.* **431** 29–33
[76] Jirage K B, Hulteen J C and Martin C R 1997 Nanotubule-based molecular-filtration membranes *Science* **278** 655–8
[77] Semiconductor Industry Association 2001 *International Technology Roadmap for Semiconductors* (Austin, TX: Semiconductor Industry Association)
[78] Barcilon V 1992 Ion flow through narrow membrane channels: part I *SIAM J. Appl. Math.* **52** 1391–404
[79] Barcilon V, Chen D P and Eisenberg R S 1992 Ion flow through narrow membrane channels: part II *SIAM J. Appl. Math.* **52** 1405–25
[80] Chen D P, Barcilon V and Eisenberg R S 1992 Constant fields and constant gradients in open ionic channels *Biophys. J.* **61** 1372–93
[81] Jordan P C *et al* 1989 How electrolyte shielding influences the electrical potential in transmembrane ion channels *Biophys. J.* **55** 1041–52
[82] Levitt D G 1985 Strong electrolyte continuum theory solution for equilibrium profiles, diffusion limitation, and conductance in charged ion channels *Biophys. J.* **48** 19–31
[83] Peskoff A and Bers D M 1988 Electrodiffusion of ions approaching the mouth of a conducting membrane channel *Biophys. J.* **53** 863–75
[84] Schumaker M F and Kentler C J 1998 Far-field analysis of coupled bulk and boundary layer diffusion toward an ion channel entrance *Biophys. J.* **74** 2235–48
[85] Corry B *et al* 2002 Reservoir boundaries in Brownian dynamics simulations of ion channels *Biophys. J.* **82** 1975–84
[86] Corry B, Kuyucak S and Chung S-H 2000 Invalidity of continuum theories of electrolytes in nanopores *Chem. Phys. Lett.* **320** 35–41
[87] Corry B, Kuyucak S and Chung S-H 2000 Tests of continuum theories as models of ion channels: II. Poisson–Nernst–Planck theory versus Brownian dynamics *Biophys. J.* **78** 2364–81
[88] Moy G *et al* 2000 Tests of continuum theories as models of ion channels: I. Poisson–Boltzmann theory versus Brownian dynamics *Biophys. J.* **78** 2349–63
[89] Dieckmann G R *et al* 1999 Exploration of the structural features defining the conduction properties of a synthetic ion channel *Biophys. J.* **76** 618–30
[90] Lo W Y *et al* 1998 Molecular simulation of electrolytes in nanopores *J. Electroanal. Chem.* **450** 265–72
[91] Sung W and Park P J 1996 Polymer translocation through a pore in a membrane *Phys. Rev. Lett.* **77** 783–6
[92] Lubensky D K and Nelson D R 1999 Driven polymer translocation through a narrow pore *Biophys. J.* **77** 1824–38
[93] Muthukumar M 1999 Polymer translocation through a hole *J. Chem. Phys.* **111** 10371–4
[94] Muthukumar M 2002 Theory of sequence effects on DNA translocation through proteins and nanopores *Electrophoresis* **23** 1417–20
[95] de Gennes P-G 1999 Passive entry of a DNA molecule into a small pore *Proc. Natl Acad. Sci. USA* **96** 7262–4
[96] Park P J and Sung W 1998 Polymer release out of a spherical vesicle through a pore *Phys. Rev.* E **57** 730–4
[97] Muthukumar M 2001 Translocation of a confined polymer through a hole *Phys. Rev. Lett.* **86** 3188–91
[98] Kumar K K and Sebastian K L 2000 Adsorption-assisted translocation of a chain molecule through a pore *Phys. Rev.* E **62** 7536–9
[99] Park P J and Sung W 1998 Polymer translocation induced by adsorption *J. Chem. Phys.* **108** 3013–18
[100] Baumgartner A and Skolnick J 1995 Spontaneous translocation of a polymer across a curved membrane *Phys. Rev. Lett.* **74** 2142–5
[101] Liu S and Muthukumar M 2002 Langevin dynamics simulation of counterion distribution around isolated flexible polyelectrolyte chains *J. Chem. Phys.* **116** 9975–82

[102] Mercier J-F and Slater G W 1999 Numerically exact diffusion coefficients for lattice systems with periodic boundary conditions: II. Numerical approach and applications *J. Chem. Phys.* **110** 6057–65
[103] Viovy J L 2000 Electrophoresis of DNA and other polyelectrolytes: physical mechanisms *Rev. Mod. Phys.* **72** 813–72
[104] Kong C Y and Muthukumar M 1998 Monte Carlo study of adsorption of a polyelectrolyte onto charged surfaces *J. Chem. Phys.* **109** 1522–7
[105] Chern S-S, Cardenas A E and Coalson R D 2001 Three-dimensional dynamic Monte Carlo simulations of driven polymer transport through a hole in a wall *J. Chem. Phys.* **115** 7772–82
[106] Baumgartner A 1980 Statics and dynamics of the freely jointed polymer chain with Lennard-Jones interaction *J. Chem. Phys.* **72** 871–9
[107] Bates M, Burns M and Meller A 2003 Dynamics of DNA molecules in a membrane channel probed by active control techniques *Biophys. J.* **84** 2366–72
[108] Saleh O A and Sohn L L 2003 An artificial nanopore for molecular sensing *Nano Lett.* **3** 37–8
[109] SantaLucia J 1995 A unified view of polymer, dumbbell, and oligonucleotide DNA nearest-neighbor thermodynamics *Proc. Natl Acad. Sci. USA* **95** 1460–5
[110] Storm A J, van den Broek D, Lemay S and Dekker C 2002 Solid-state nanopores for single-molecule DNA studies *Biophys. J.* **82** 256
[111] Slonkina E and Kolomeisky A B 2003 Polymer translocation through a long nanopore *J. Chem. Phys.* **118** 7112–18
[112] Ambjörnsson T, Apell S P, Konkoli Z, Di Marzio E A and Kasianowicz J J 2002 Charged polymer membrane translocation *J. Chem. Phys.* **117** 4063–73
[113] Meller A 2003 Dynamics of polynucleotide transport through nanometer-scale pores *J. Phys.: Condens. Matter* **15** 581–607